ACS APPLIED MATERIALS & INTERFACES

Research Article

www.acsami.org

Interfaces in Nano-/Microcrystalline Multigrade CVD Diamond Coatings

Flávia A. Almeida,*[,†] Ermelinda Salgueiredo,[†] Filipe J. Oliveira,[†] Rui F. Silva,[†] Daniel L. Baptista,[‡,§] Suzana B. Peripolli,[∥] and Carlos A. Achete[‡]

[†]Department of Materials and Ceramic Engineering, CICECO, University of Aveiro, 3810-193 Aveiro, Portugal

[‡]Divisão de Metrologia de Materiais - DIMAT, Inmetro, Av. Nossa Senhora das Graças 50, Xerém, Duque de Caxias, Rio de Janeiro, 25250-020, Brazil

[§]PPGMicro - Instituto de Física, Universidade Federal do Rio Grande do Sul, PortoAlegre, Rio Grande do Sul, 91501-970, Brazil

[∥]Centro de Tecnologia SENAI Solda, Rua São Francisco Xavier, 601, Maracanã, Rio de Janeiro, 20550-011, Brazil

ABSTRACT: The interfaces of multilayered CVD diamond films grown by the hot-filament technique were characterized with high detail using HRTEM, STEM-EDX, and EELS. The results show that at the transition from micro- (MCD) to nanocrystalline diamond (NCD), a thin precursor graphitic film is formed, irrespectively of the NCD gas chemistry used (with or without argon). On the contrary, the transition of the NCD to MCD grade is free of carbon structures other than diamond, the result of a higher substrate temperature and more abundant atomic H in the gas chemistry. At those transitions WC nanoparticles could be found due to contamination from the filament, being also present at the first interface of the MCD layer with the silicon nitride substrate.

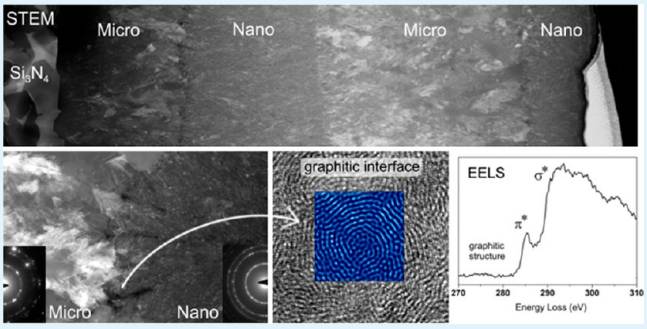

KEYWORDS: *CVD diamond, multilayer, interface, high resolution transmission electron microscopy*

1. INTRODUCTION

Chemically vapor deposited (CVD) diamond coatings are used in wear resistant parts for demanding mechanical and tribological solicitations, due to properties such as high hardness and elastic modulus, chemical inertness, and low self-friction coefficient. Microcrystalline diamond (MCD) grades ensure higher adhesion to suitable substrates, like silicon nitride (Si_3N_4) ceramics, when compared to nanocrystalline diamond (NCD) coatings.[1,2] Also, the hardness and Young's modulus values of NCD are slightly lower than those of MCD, which is attributed to the presence of sp^2 amorphous carbon phases incorporated at the grain boundaries.[3] However, the evolutionary crystal growth mechanism of MCD results in the increase of the crystal size with thickness and thus of the surface roughness.[4] This has a negative effect in the behavior of cutting tools and components subjected to tribological contact, such as mechanical seals or drawing dies, by increasing the wear rates and the initial friction coefficients, compromising the efficiency and quality of the products.[5−7] Contrarily, the continuous renucleation process of the NCD film ensures an even crystallite size along the thickness, resulting in very smooth ending surfaces, ready for tribological applications.[8]

By combining the advantages of each type of diamond coating grade, while simultaneously minimizing their limitations, multilayered multigrade CVD diamond coatings are a promising solution to improve the tribological performance. In an earlier work,[9] high resolution transmission electron microscopy (HRTEM) and electron energy loss spectroscopy (EELS) characterization were crucial to fully understand the nature of the interface between monolayer MCD films and Si_3N_4 ceramic substrates. The formation of a diamond-like carbon interlayer was detected and, to a lesser extent, grain-to-grain direct transition of diamond to Si_3N_4 crystals with a 8.2° misorientation angle was demonstrated. So far, to our knowledge, the only study of interfaces using HRTEM within a multilayer coating, i.e., between diamond layers, is the work of Jiang and co-workers.[10] They characterized a bilayered MCD/NCD diamond coating on silicon substrates grown using a microwave plasma CVD reactor, assisted by a negative bias for NCD growth. At the MCD/NCD interface region, a local lattice distortion was observed within a range of several angstroms. They supposed that such a feature was induced by the negative bias application, by creating energetic ion bombardment to the diamond growing facets, which locally caused diamond lattice distortions. The subsequent insertion of C atoms did not follow the original crystallographic orientation, resulting in the secondary nucleation of NCD crystals.

Received: August 14, 2013
Accepted: October 28, 2013
Published: October 28, 2013

Table 1. Deposition Conditions of the Different Diamond Grades in the HFCVD Reactor

	CH_4/H_2 ratio	Ar/H_2 ratio	gas flow (sccm)	total pressure (kPa)	substrate temperature (°C)	growth rate ($\mu m \cdot h^{-1}$)
filament carburization	0.026	-	200	10.0	630	-
MCD	0.026	-	100	17.5	800	1.7
NCD-(Ar)	0.04	0.1	200	10.0	700	0.1−0.4[a]
NCD-(CH_4)	0.073	-	100	5.0	700	1.2

[a]Depending on whether it is a continuous or interrupted deposition procedure.

In the present work, 4-fold multilayered MCD/NCD multigrade diamond coatings were grown by hot filament chemical vapor deposition (HFCVD) technique. Very recently, it was shown that the interfaces between the two diamond types play an important role on the mechanical response of those multilayer structures.[11,12] The superior erosion behavior of the diamond multigrade coatings was attributed to the action of the MCD/NCD interfaces in deflecting cracks, thus acting as "energy sinks" to further crack propagation. Besides improved mechanical response, optical and electrical properties can also be influenced by the presence of impurities, porosity, nondiamond carbon content and other structural aspects at the MCD/NCD interfaces. The study of these features and their correlation with the deposition processes are the main subjects of the present paper and can be beneficial to tailor the properties for other applications, such as micro-electrical mechanical systems, sensors, and energy devices. It is thus imperative to carefully observe the diamond interfaces by high resolution electron microscopy and spectroscopic techniques. The knowledge of how the different layers and diamond grades connect to each other and the possible formation of graphitic interlayers are some of the questions to be answered. A detailed study of interfaces using high resolution transmission electron microscopy (HRTEM) and scanning TEM (STEM), coupled with electron energy-loss spectroscopy (EELS), is hereby presented.

2. EXPERIMENTAL SECTION

Fourfold multilayered MCD/NCD multigrade coatings were grown by hot filament chemical vapor deposition (HFCVD), starting with a first layer of adherent MCD onto the Si_3N_4 ceramic substrate and finishing with a smooth NCD top layer. Prior to diamond deposition all substrates were ultrasonically seeded during 1 h with a nanometric diamond (4−6 nm) powder suspension in ethanol, for diamond nucleation enhancement. One type of MCD and two types of NCD layers were involved. The deposition conditions of each layer are given in Table 1 together with the filament carburization mode. The NCD diamond growth parameters differ from those of MCD first on the lower substrate temperature and, mainly, on the strategies used for enhancing diamond renucleation: (i) in the case of the NCD-(CH_4) grade, it is achieved by carbon supersaturation coming from a high methane (CH_4) concentration; (ii) for the NCD-(Ar) grade, besides a methane rich gas phase, the partial replacement of hydrogen (H_2) by argon (Ar) in the gas composition also contributes for the increased diamond renucleation.

Three types of diamond multilayers were designed: (i) Multi-A, consisting of a fourfold MCD/NCD-(Ar)/MCD/NCD-(Ar) stacking performed in one single deposition step, by switching the deposition parameters without venting the reactor; (ii) Multi-B, grown as Multi-A but with the NCD-(CH_4) grade replacing NCD-(Ar); and (iii) Multi-C, grown using the same deposition parameters of Multi-A but interrupting the process after each deposited layer to vent the reactor and to replace the tungsten filaments.

Diamond deposition was conducted in an in-house built 3 kW HFCVD reactor. Six tungsten wires (Ø = 0.25 mm, 75 mm length) were placed at a constant distance of ~7 mm from the substrate. The filament temperature was measured with a two-color pyrometer (Raytek) and kept constant at about 2300 °C, while the substrate temperature was assessed by a K-type thermocouple inserted into the substrate holder, contacting the bottom face of the substrate. The samples were heated to approximately 630 °C by thermal radiation, and additional heating was provided by a graphite dissipating element for full temperature control.

The cross-sectional preparation of well-preserved interfaces for HRTEM/EELS characterization was only possible using the focused ion beam (FIB) technique (FEI Nova Nanolab 600), following an earlier optimized preparation protocol.[9] HRTEM and scanning TEM (STEM), coupled with EELS, were accomplished in a FEI Titan 80/300 apparatus equipped with a Gatan imaging filter Tridiem.

3. RESULTS AND DISCUSSION

A general cross-section view of Multi-A coating is given in the conventional transmission electron microscopy (CTEM) micrograph of Figure 1a, in bright field mode, where the

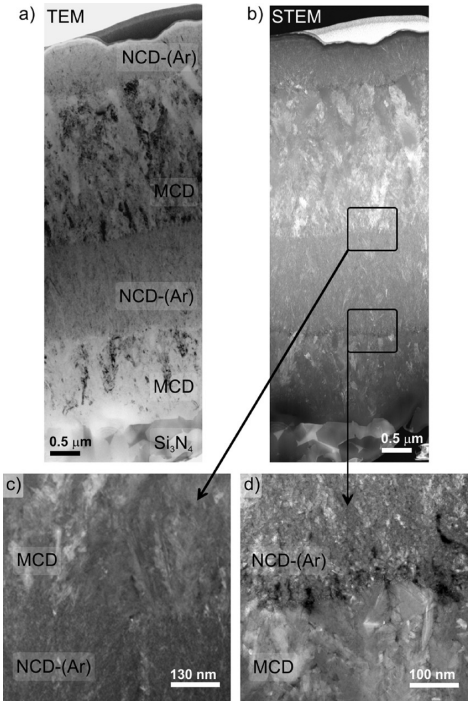

Figure 1. Cross-sectional view of Multi-A sample: (a) bright field mode CTEM micrograph; (b) same region in HAADF-STEM mode; and (c) and (d) high magnifications of the NCD-(Ar)/MCD and MCD/NCD-(Ar) transitions, respectively.

different layers are delimited by net interfaces, corresponding to the transitions between the diamond grades. The Si_3N_4 substrate is evident at the bottom, well-defined by the faceted Si_3N_4 grains. Figure 1b is an image of scanning transmission electron microscopy in high angle annular dark field (STEM-HAADF) of the same region of Figure 1a, and it highlights the larger, micrometric, diamond crystals in the case of MCD layer, in contrast to the nanometric crystals of the NCD-(Ar) layers.

In the case of MCD, grains form perpendicularly to the substrate, while in NCD-(Ar) deposition equiaxed crystallites grow. These features are better visualized in the higher magnifications images of Figure 1c,d. Furthermore, the Z-contrast imaging given by the STEM-HAADF reveals that the NCD-(Ar)/MCD and MCD/NCD-(Ar) transitions are very distinct: an abrupt interface is revealed in the former (Figure 1c), while an interphase transition appears in the latter (Figure 1d). In the MCD/NCD-(Ar) transition, approximately 50 nm thick, dark contrast nodules are visible in all extensions, corresponding to graphitic carbon.

A cross-sectional view of sample Multi-B is presented in Figure 2a and by the superposition of Figure 2b (after sample thinning). No significant differences could be found in the nature of the interfaces relatively to those of Multi-A coatings. The higher magnification HRTEM image in Figure 2c emphasizes the structure of the dark contrast nodules that appear in the MCD/NCD transition zone of both types of coatings. Straight and wavy fringes of graphite-like structures are visible as well as some loop formation of graphite sheets, where there is no stacking order between adjacent graphene planes, typical of disordered turbostratic graphite.[13] Their graphitic character is confirmed by the interplanar measurement of the inverse fast Fourier transform (IFFT) filtered image (inset of Figure 2c) and electron energy loss spectroscopy (EELS) (inset of Figure 2a,b).

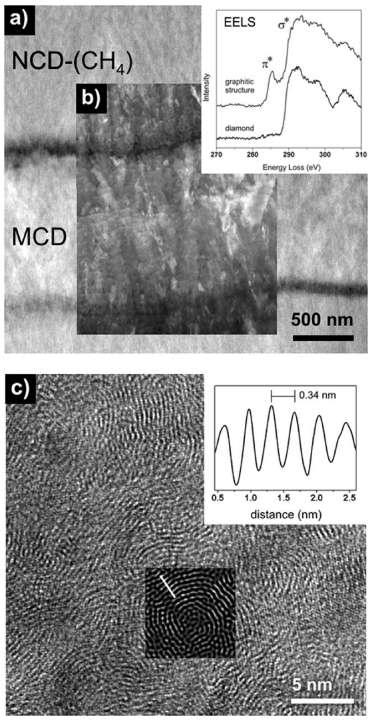

Figure 2. (a) Cross-sectional view of Multi-B sample; (b) superposition after sample thinning; (c) higher magnification of the black nodules in MCD/NCD transition. Insets in (a) and (b): electron energy loss spectroscopy (EELS) of the MCD/NCD-(CH_4) interface region. Inset in (c): inverse fast Fourier transform (IFFT) of the black nodules in that region, showing their graphitic character.

During the different diamond coating transitions, several time-dependent events take place: (i) change of chamber pressure by a few seconds of purge, (ii) introduction of the new gas mixture, (iii) stabilization of new pressure value; (iv) fluctuation of filament and substrate temperatures; and (v) new gas composition under equilibrium. Some minutes are necessary for the stabilization of growth conditions, where graphite deposition may take place as shown above in Figure 1d and Figure 2. This graphitic phase appears only in the transition from MCD to NCD deposition conditions, most likely due to a combined effect of a lower deposition temperature of NCD and the lower amount of H_2 supplied in the gas mixture (Table 1). It is well-known that there is a competition between the sp^2 and sp^3 carbon deposition during CVD diamond growth, where the atomic H plays a decisive etching role of the graphitic phases.[14] During that transition and before the NCD growth surface is established, the atomic H content decreases to a level that is not sufficient for total removal of the graphitic phases. A progressive transition from MCD to NCD growth conditions would prevent the formation and stabilization of graphite.

Spatially localized STEM-EELS spectra in the inset of Figure 2a,b present both 1s $\rightarrow$ σ^* and 1s $\rightarrow$ π^* C electronic transitions, at around 289 and 285 eV, respectively. The spectrum of crystallites from the bulk NCD region shows only the typical diamond σ^* peaks, indicating a good quality of the diamond nanocrystals. Hoffman et al.[15] observed the formation of a thin precursor graphitic film on silicon followed by the deposition of a film of diamond character as a function of substrate temperature in the direct current glow discharge (DCGD) CVD method. They determined that at a certain temperature (of about 880 °C in that case), the evolution of local stresses reached a maximum value, suggesting that it is the relaxation of these stresses that leads to the transformation of the graphitic material into the nanodiamond phase. Thus, the stabilization of the diamond phase would be given by the hydrogen adsorption/desorption process in the nucleation and growth of the nanocrystalline diamond films in a narrow range of temperatures. It is worth noting that in the NCD-(Ar)/MCD transition (Figure 1b,c), when MCD deposition conditions are imposed and graphitic phases form, the higher substrate temperature and more abundant atomic H do not allow these phases to survive the subsequent diamond growth.

Figure 3a is a magnified STEM-HAADF micrograph of the MCD/NCD-(Ar) interface region, showing white contrast nanoparticles, also present between the Si_3N_4 substrate and the first MCD layer (Figure 3b), though these particles were never found inside the diamond layers. Energy dispersive X-ray (STEM-EDX) analysis (Figure 3c) of that region shows the characteristic L and M peaks of tungsten that can only be due to contamination from the filament.

It is well-known that contamination of the coating by tungsten from filament vaporization can happen, even when the filaments are previously carburized for long periods of time.[16−18] Neto et al.[19] used this phenomenon to produce bilayered coatings of diamond/WC over Si in a hot filament reactor starting with a W film. In the present work, tungsten carbide nanoparticles at the MCD/NCD-(Ar) (Figure 3a) and Si_3N_4/MCD (Figure 3b) interfaces could only be visualized at high magnifications under TEM/STEM and for carefully prepared samples.

The filament carburization step before the growth of the first MCD layer is carried out with the Si_3N_4 substrates inside the reactor, so W vaporization from the filament occurs before an outer layer of W_2C can be formed. This probably explains why larger nanoparticles (5−10 nm) are found at the Si_3N_4/MCD transition (Figure 3b) than at the MCD/NCD-(Ar) ones (~ 3 nm, Figure 3a). The last diamond layer transition is from MCD

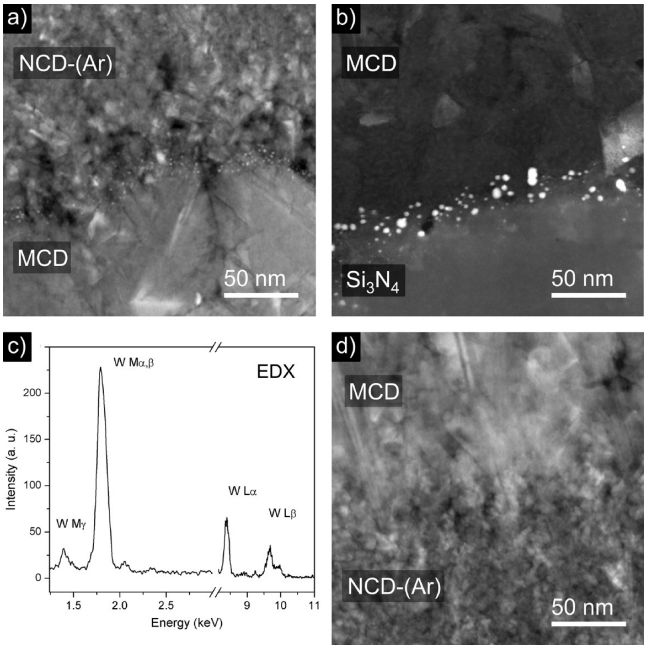

Figure 3. Interfaces details of Multi-A sample: (a) STEM-HAADF micrograph of the MCD/NCD-(Ar) interface region and (b) of the Si_3N_4/MCD interface region. (c) Energy dispersive X-ray (STEM-EDX) analysis showing the characteristic L and M peaks of tungsten. (d) STEM-HAADF micrograph of the NCD-(Ar)/MCD interface region.

to NCD grade, where the tungsten carbide nanoparticles are more easily found than in the case of NCD to MCD switching, as seen in the high magnification of Figure 3d. This phenomenon happened irrespectively of the NCD growth condition, whether by Ar addition (Multi-A coating) or CH_4 supersaturation (Multi-B one). In the case of MCD to NCD transition, an abrupt increase of the filament temperature occurs (to ~2500 °C) when adding larger quantities of CH_4 and/or Ar to the reactor. This compels a rapid adjustment of the total current in order to maintain the temperature range of deposition (54A in the case of MCD, 50A for NCD-(CH_4), and 48A for NCD-(Ar) depositions, for six filaments). This temperature increase probably causes WC dissociation, as reported in the work of Menon et al.,[17] leaving W vulnerable to vaporization before carburization restarts under moderate filament temperatures. Nevertheless, tungsten vaporization is likely to happen in a few instants, as no noticeable amount of WC nanoparticles is found throughout the cross section of the NCD films. Moreover, a "poisoning" or "sooting" effect of graphitic deposition at the filament surface occurs, especially in the case of Multi-A coating (with Ar addition). These graphitic depositions reduce the number of active sites available for the H_2 decomposition reactions,[20,21] accounting for the decrease of growth rate and renucleation effects of the NCD films with time. Inspection of the filaments after the deposition of Multi-A coatings showed the formation of a thick and stable carbon layer around them, with the same aspect as the one found in the work of May et al.,[22] which is responsible for the stopping of the diamond film growth. However, by venting the reactor and renewing the tungsten filaments after the deposition of each diamond layer, this drawback could be easily overcome in the growth of Multi-C samples. In the case of Multi-C films, large WC nanoparticles, such as those seen at the Si_3N_4/MCD interface for the other samples, are visible in all the diamond transition regions (Figure 4). Graphitic phases, especially at the MCD/NCD transition, also form as in the Multi-A and Multi-B samples.

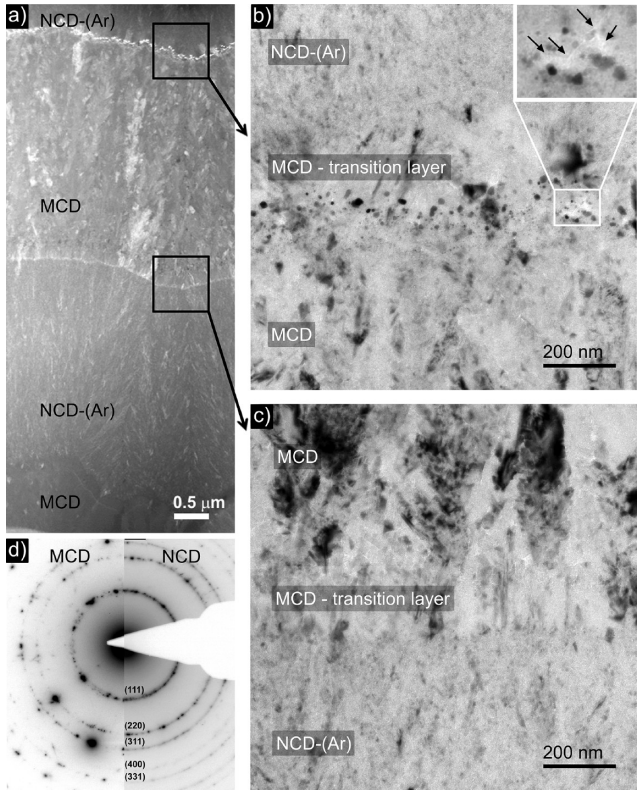

Figure 4. Cross-sectional view of the Multi-C sample: (a) general view of the different diamond interfaces in STEM mode; (b) and (c) CTEM micrograph of the MCD/NCD-(Ar) and NCD-(Ar)/MCD transitions, respectively; and (d) selected-area electron diffraction (SAED) overlap projections of both diamond grades.

The micrograph of Figure 4b presents the region between the first MCD and the subsequent first NCD film, where a transition layer is clearly marked by the WC nanoparticles. This transition layer, approximately 150 nm thick, develops during the 10 min of carburization. Although during this stage the filaments consume C from the reactive species, the previous MCD layer continues to grow until the deposition condition changed fully to the NCD one. This feature also happens in the NCD/MCD interface, where a MCD transition layer (formed during carburization) is recognizable below the MCD coating, formed during the growth step (Figure 4c).

The crystallographic analysis of the diamond layers is given in Figure 4d, in the form of overlapping selected-area electron diffraction (SAED) projections of both diamond grades. Sharp Bragg reflection spots are visible at the left-hand side, in the case of MCD, and sharp ring patterns are visible at the right-hand side of Figure 4d, for the NCD-(Ar) layer; the latter being indicative of the randomness of the crystallite orientation. All the SAED patterns correspond to the diamond (111), (220), (311), (222), (400), and (331) planes, from inner to outer rings, respectively.

This detailed characterization of the different types of interfaces helps reinforcing the conclusions of two recently published papers on the mechanical performance of these multilayer coatings under erosive wear[11] and in reciprocating

dry contacts.[12] Particularly, in the first paper, interfacial failure is clearly revealed at the transition between MCD and the top NCD layer. The combined role of graphitic and WC nanoparticles contributed in fact to enhance the erosion resistance by acting as an "energy sink" toughening mechanism to the further development of cracks into the substrate/diamond interface region. As a result, the induction time to film delamination under SiC particles impact more than duplicates in the case of multilayer coatings compared to diamond monolayers. For the tribological tests, it was found that these composite coatings exhibit a critical load before delamination (130−200 N) much larger than mono- (60−100 N) or even bilayer coatings (110 N), for films of the same thickness (∼10 μm). This was accompanied by a progressive wear of the NCD top layer that acted sacrificially, while the harder microcrystalline diamond layer kept the residual stresses at lower levels.

4. CONCLUSIONS

Multilayered MCD/NCD diamond coatings have been successfully grown by hot-filament CVD using continuous and discontinuous approaches. Three different multigrade diamond films were obtained, by changing the deposition parameters of the nanocrystalline diamond (with or without argon) and the transition mode between the diamond grades (continuously or venting the reactor after each layer deposition and changing the tungsten filaments). Cross-sectional samples, with well-preserved interfaces, were prepared by FIB and were successfully characterized by means of HRTEM, STEM-EDX, and EELS techniques.

The interface between the diamond layers depends on the switching order: from MCD to NCD or from NCD to MCD. In the former, the transition is characterized by the formation of graphite-like structures, as confirmed by the more prominent π^* C peak at 285 eV in spatially resolved STEM-EELS. The higher carbon content (and lower H concentration) of both NCD growth parameters allowed the formation of those sp^2 structures. This occurs before stabilization of the hydrogen adsorption/desorption process allows the nucleation of the diamond phase. On the contrary, the transition from the NCD to MCD grade is free of carbon structures other than diamond. In this case, the more abundant atomic H of the MCD deposition conditions does not allow the sp^2 phases to survive etching.

Another common feature found in all the interfaces of MCD to NCD transitions, for both kinds of NCD, is the presence of nanometric round-shaped particles of tungsten carbide, which arise from filament contamination. At this transition, the parameters imposed to grow the NCD crystals (higher CH_4 concentration and/or argon addition) increase considerably the filament temperature, probably dissociating the carburized layer around the filament and leaving W vulnerable to vaporize.

The addition of argon also changes the filament structure, creating a thick and stable carbon layer around it. This causes the loss of filament efficiency, decreasing the diamond film growth rate. So, when using argon to perform the NCD layer of a multilayered diamond film, aiming for a well-controlled layer thickness, the discontinuous process of stopping the deposition and replacing the filaments was shown to be a better solution for the NCD-Ar coatings.

AUTHOR INFORMATION

Corresponding Author

*E-mail: falmeida@ua.pt.

Notes

The authors declare no competing financial interest.

ACKNOWLEDGMENTS

Brazil/Portugal collaboration was undertaken under CNPq project no. 402251/2012-1 "Nanostructured carbon allotropes". F.A.A. and E.S. acknowledge FCT for Grants SFRH/BPD/34869/2007 and SFRH/BD/41757/2007, respectively. The authors acknowledge Foundation for Science and Technology (FCT, Portugal) for funding the projects MULTIDIACOAT PTDC/EME-TME/100689/2008 and PEst-C/CTM/LA0011/2013.

REFERENCES

(1) Almeida, F. A.; Amaral, M.; Oliveira, F. J.; Fernandes, A. J. S.; Silva, R. F. *Vacuum* **2007**, *81*, 1443−1447.
(2) Abreu, C. S.; Amaral, M. S.; Fernandes, A. J. S.; Oliveira, F. J.; Silva, R. F.; Gomes, J. R. *Diamond Relat. Mater.* **2006**, *15*, 739−744.
(3) Catledge, S. A.; Borham, J.; Vohra, Y. K.; Lacefield, W. R.; Lemons, J. E. *J. Appl. Phys.* **2002**, *91*, 5347−5352.
(4) Kulisch, W.; Popov, C. *Phys. Status Solidi A* **2006**, *203*, 203−219.
(5) Almeida, F. A.; Amaral, M.; Oliveira, F. J.; Silva, R. F. *Diamond Relat. Mater.* **2006**, *15*, 2029−2034.
(6) Mubarok, F.; Carrapichano, J. M.; Almeida, F. A.; Fernandes, A. J. S.; Silva, R. F. *Diamond Relat. Mater.* **2008**, *17*, 1132−1136.
(7) Sun, F.; Ma, Y.; Shen, B.; Zhang, Z.; Chen, M. *Diamond Relat. Mater.* **2009**, *18*, 276−282.
(8) Gruen, D. M. *Annu. Rev. Mater. Sci.* **1999**, *29*, 211−259.
(9) Almeida, F. A.; Oliveira, F. J.; Silva, R. F.; Baptista, D. L.; Peripolli, S. B.; Achete, C. A. *Appl. Phys. Lett.* **2011**, *98*, 171913−1−171913−3.
(10) Jiang, N.; Sugimoto, K.; Nishimura, K.; Shintani, Y.; Hiraki, A. *J. Cryst. Growth* **2002**, *242*, 362−366.
(11) Salgueiredo, E.; Almeida, F. A.; Amaral, M.; Neto, M. A.; Oliveira, F. J.; Silva, R. F. *Wear* **2013**, *297*, 1064−1073.
(12) Salgueiredo, E.; Abreu, C. S.; Amaral, M.; Oliveira, F. J.; Gomes, J. R.; Silva, R. F. *Wear* **2013**, *303*, 225−234.
(13) Pimenta, M. A.; Dresselhaus, G.; Dresselhaus, M. S.; Cançado, L. G.; Jorio, A.; Saito, R. *Phys. Chem. Chem. Phys.* **2007**, *9*, 1276−1291.
(14) Frenklach, M. In *Diamond and diamond-like films and coatings*; Clausing, R. E., Horton, L. L., Angus, J. C., Koidl, P., Eds.; Plenum Press: New York, 1991; p 499.
(15) Hoffman, A.; Heiman, A.; Strunk, H. P.; Christiansen, S. H. *J. Appl. Phys.* **2002**, *91*, 3336−3344.
(16) Zeiler, E.; Schwarz, S.; Rosiwal, S. M.; Singer, R. F. *Mater. Sci. Eng., A* **2002**, *335*, 236−245.
(17) Menon, P. M.; Edwards, A.; Feigerle, C. S.; Shaw, R. W.; Coffey, D. W.; Heatherly, L.; Clausing, R. E.; Robinson, L.; Glasgow, D. C. *Diamond Relat. Mater.* **1999**, *8*, 101−109.
(18) Contreras, O.; Hirata, G. A.; Avalos-Borja, M. *Appl. Surf. Sci.* **2000**, *158*, 236−245.
(19) Neto, M. A.; Silva, E. L.; Fernandes, A. J. S.; Oliveira, F. J.; Silva, R. F. *Surf. Coat. Technol.* **2012**, *206*, 3055−3063.
(20) Dandy, D.; Coltrin, M. E. *J. Appl. Phys.* **1994**, *76*, 3102−3113.
(21) Yehoda, J. E. In *Diamond Films Handbook*; Asmussen, J., Reinhard, D. K., Eds.; Marcel Dekker: New York, 2001; p 119.
(22) May, P. W.; Smith, J. A.; Mankelevich, Y. A. *Diamond Relat. Mater.* **2006**, *15*, 345−352.